Chapter

Water Waves and Light: Two Unlikely Partners

Georgios N. Koutsokostas, Theodoros P. Horikis, Dimitrios J. Frantzeskakis, Nalan Antar and İlkay Bakırtaş

Abstract

We study a generic model governing optical beam propagation in media featuring a nonlocal nonlinear response, namely a two-dimensional defocusing nonlocal nonlinear Schrödinger (NLS) model. Using a framework of multiscale expansions, the NLS model is reduced first to a bidirectional model, namely a Boussinesq or a Benney-Luke-type equation, and then to the unidirectional Kadomtsev-Petviashvili (KP) equation – both in Cartesian and cylindrical geometry. All the above models arise in the description of shallow water waves, and their solutions are used for the construction of relevant soliton solutions of the nonlocal NLS. Thus, the connection between water wave and nonlinear optics models suggests that patterns of water may indeed exist in light. We show that the NLS model supports intricate patterns that emerge from interactions between soliton stripes, as well as lump and ring solitons, similarly to the situation occurring in shallow water.

Keywords: Kadomtsev-Petviashvili equation, nonlocal nonlinear Schrödinger equation, line solitons, soliton interactions, lump solitons, patterns of light

1. Introduction

For many decades, solitons, namely robust localized waveforms that propagate undistorted in nonlinear dispersive media, have been a topic of particular interest in physics [1, 2] and applied mathematics [3, 4]. These waveforms have a variety of fascinating properties that should be mentioned: due to their particle-like nature, solitons collide elastically, thus preserving their shape after the collision process. In some cases, as e.g. in shallow water, line soliton collisions give rise to the emergence of various wave patterns, including X-, H-, or Y-shaped waves, as well as other, even more complicated, waveforms – see, e.g., Ref. [5] for a set of remarkable examples and observations. Such patterns can be described by multidimensional line soliton solutions of the Kadomtsev-Petviashvili II (KPII) equation, a variant of the KP equation [6] with negative dispersion – as is the case of water waves with small surface tension. In particular, the KP equation can be expressed as:

$$\frac{\partial}{\partial x}\left(\frac{\partial u}{\partial t}+6u\frac{\partial u}{\partial x}+\frac{\partial^3 u}{\partial x^3}\right)+3\sigma\frac{\partial^2 u}{\partial y^2}=0, \tag{1}$$

where $\sigma=\pm1$: for $\sigma=+1$ (negative dispersion/small surface tension) Eq. (1) is a KPII, while for $\sigma=-1$ (positive dispersion/large surface tension) Eq. (1) is a KPI.

We should mention that both versions of the KP belong to the – rather limited – class of completely integrable equations in $(2+1)$-dimensions [3].

Important to the collision-induced emergence of different types of wave patterns in shallow water is the fact that quasi (line) solitons of the KPII are stable. Furthermore, of paramount importance is the effect of soliton resonances [7–10], whereby two (or more) colliding solitons resonate under certain conditions, thus creating novel stable structures. It is, thus, not surprising that the collision dynamics of many robust solitons, can give rise to a wealth of complex wave patterns [11–16] (see also [1]).

The above discussion motivates the following question: can solitons, similar to those governed by the KPII equation and feature rich collision dynamics (as in shallow water waves), be also predicted – and, possibly, observed – in nonlinear optics? In this context, key model is the nonlinear Schrödinger (NLS) equation, which is known to support soliton solutions (see, e.g., Ref. [17] and references therein). As was shown some time ago [18], the $(2+1)$-dimensional defocusing NLS can be asymptotically reduced to the KPI equation, which allows one to approximate dark soliton stripes of the NLS as line solitons of KPI; then, the fact that line KPI solitons are unstable [3], can be used to investigate the transverse instability of dark solitons [18–20]. On the other hand, as was recently shown [21], the presence of nonlocality introduces an effective *surface tension* in the system. Then, in the case where the surface tension is small – corresponding to the case of *strong nonlocality* – it can be shown that the nonlocal NLS model can be asymptotically reduced to a *KPII equation*. This result allows for the derivation of approximate *stable* line soliton solutions of the nonlocal NLS, which behave similarly to the stable line solitons of KPII, i.e., they undergo elastic collisions and form patterns similar to those observed in shallow water.

The scope of this work is to review the above ideas and present a variety of soliton solutions and their dynamics in the framework of a defocusing nonlocal NLS model. These solutions stem from the soliton solutions of KP models, which are derived from the nonlocal NLS via a two-step multiscale expansion method. We show that, similarly to the water wave case, the nonlocal NLS can also support complicated wave patterns, arising from "complex interactions" between two or more antidark soliton stripes that are supported in the strong nonlocality regime. In addition, we present other soliton solutions, namely dark lumps (pertinent to the KPI equation), as well as ring dark and antidark solitons (pertinent to the cylindrical KP (cKP), *alias* Johnson's Equation [22, 23]). In particular, a summary of our main results, as well as the organization of this work, are as follows.

First, in Section 2, we introduce the nonlocal NLS model, present its continuous-wave (cw) solution, and study its stability. Then, we perform a two-step multiscale analysis. First, at an intermediate stage, we derive a Boussinesq – or a Benney-Luke (BL) [24] – type equation, which is a long-wave, multi-dimensional and bi-directional, shallow water wave model. Then, from the Boussinesq/BL-type equation, we derive its far field, pertinent to the long time behavior, which is the KP equation, both in Cartesian and in cylindrical geometry. The reduction to the KP model allows us to construct approximate soliton solutions of the nonlocal NLS, which are presented in Section 3. In the strong nonlocality regime, we derive antidark soliton stripes, satisfying an effective KPII equation, which are shown to form patterns similar to those observed in shallow water; these include X-, Y, and H-shaped waveforms, as well as other complicated patterns arising from resonant interactions between more than two solitons. We also present dark lump solitons, as well as ring dark and antidark soliton solutions of the NLS, which are numerically found to propagate undistorted in the framework of the NLS model. Finally, in Section 4, we briefly discuss the conclusions of this work.

2. Nonlocal NLS and multiscale analysis

2.1 Introduction of the model and linear regime

The model under consideration is a two-dimensional (2D) defocusing NLS, with a nonlocal nonlinearity, which is expressed in the following dimensionless form:

$$\mathrm{i}u_t + \frac{1}{2}\Delta u - nu = 0, \tag{2}$$

$$d\Delta n - n + |u|^2 = 0. \tag{3}$$

where subscripts denote partial derivatives, $u \in \mathbb{C}$, $n \in \mathbb{R}$,

$$\Delta \equiv \partial_x^2 + \partial_y^2, \quad \text{or} \quad \Delta \equiv \frac{1}{r}\partial_r(r\partial_r) + \frac{1}{r^2}\partial_\theta^2, \tag{4}$$

is the Laplacian in Cartesian or polar coordinates respectively, while the parameter $d \in \mathbb{R}_+$ measures the degree of nonlocality (see below). The above system finds a number of physical applications. For instance, in the context of optics, this model describes the evolution of the complex electric field envelope u, via a nonlinear wave equation in the paraxial regime, coupled with a diffusion-type equation for the nonlinear correction to the refractive index n depending on the intensity $I = |u|^2$ (in this case, t represents the propagation coordinate) [25, 26]. In this context, the system (2)–(3) has been used to model experiments on liquid solutions exhibiting thermal nonlinearities [27, 28]. In addition, it has also been used in studies of plasmas (in this case, n represents the relative electron temperature perturbation) [29, 30], as well as in nematic liquid crystals (in this case, n is the optically induced angle perturbation) [31, 32].

As mentioned above, parameter d represents the degree of nonlocality: for $d = 0$, one recovers the local limit, whereby the system (2)–(3) reduces to the defocusing 2D NLS equation with a local cubic (Kerr-type) nonlinearity:

$$\mathrm{i}u_t + \frac{1}{2}\Delta u - |u|^2 u = 0, \tag{5}$$

while for $d \neq 0$, Eqs. (2) and (3) feature a spatially nonlocal nonlinearity. Notice that in our perturbative analytical approach below, d will be treated as a free parameter, of order $O(1)$, thus allowing the model to acquire an arbitrary degree of nonlocality.

Our analytical approach relies on the analysis of the hydrodynamic form of the model. This can be derived upon using the Madelung transformation:

$$u = u_0\sqrt{\rho}\exp(\mathrm{i}\phi), \tag{6}$$

where u_0 is a complex constant, while the unknown real functions ρ and ϕ denote the amplitude and phase of the field u, respectively. Substituting into Eqs. (2) and (3), we obtain the following hydrodynamical system of equations:

$$\phi_t + n + \frac{1}{2}(\nabla\phi)^2 - \frac{1}{2}\rho^{-1/2}\Delta\rho^{1/2} = 0, \tag{7}$$

$$\rho_t + \nabla\cdot(\rho\nabla\phi) = 0, \tag{8}$$

$$d\Delta n - n + |u_0|^2\rho = 0, \tag{9}$$

where $\nabla \equiv (\partial_x, \partial_y)$ or $\nabla \equiv (\partial_r, \frac{1}{r}\partial_\theta)$ is the gradient operator in Cartesian or in polar coordinates respectively.

The simplest, non trivial, solution of Eqs. (2) and (3) is of the form:

$$\rho = 1, \quad \phi = -|u_0|^2 t, \quad n = |u_0|^2, \tag{10}$$

which corresponds to the continuous wave (cw) solution $u = u_0 \exp(-\mathrm{i}|u_0|^2 t)$ and the constant function $n = |u_0|^2$. This solution will serve as a "pedestal", on top of which we will seek nonlinear excitations, namely solitons. It is thus necessary to investigate whether the solution (7) is modulationally stable. This can be done upon introducing to Eqs. (7)–(9) the following perturbation ansatz:

$$\rho = 1 + \varepsilon\tilde{\rho}, \quad \phi = -|u_0|^2 t + \varepsilon\tilde{\phi}, \quad n = |u_0|^2 + \varepsilon\tilde{n}, \tag{11}$$

where $0 < \varepsilon \ll 1$ is a formal small parameter. This way, we obtain, at $O(\varepsilon)$, the following linear system:

$$\tilde{\phi}_t + \tilde{n} - \frac{1}{4}\Delta\tilde{\rho} = 0, \tag{12}$$

$$\tilde{\rho}_t + \Delta\tilde{\phi} = 0, \tag{13}$$

$$d\Delta\tilde{n} - \tilde{n} + |u_0|^2\tilde{\rho} = 0. \tag{14}$$

The above system can straightforwardly be decoupled as follows: solving Eq. (12) for $\tilde{n}$, as well as Eq. (13) for $\Delta\tilde{\phi}$, and substituting back in Eq. (13), the following linear equation for $\tilde{\rho}$ is obtained:

$$\tilde{\rho}_{tt} - |u_0|^2\Delta\tilde{\rho} - d\Delta\tilde{\rho}_{tt} + \frac{1}{4}(1 - d\Delta)\Delta^2\tilde{\rho} = 0. \tag{15}$$

Since the above solution is linear we can examine its stability in first order by examining the dispersion relation of plane wave solutions, i.e., $\propto \exp[\mathrm{i}(\boldsymbol{k}\cdot\boldsymbol{r} - \omega t)]$, of wavenumber $k = \|\boldsymbol{k}\|$ and frequency ω (here, e.g., in Cartesian geometry, $\boldsymbol{r} = (x, y)$ and $\boldsymbol{k} = (k_x, k_y)$). Then, it can readily be found that these plane waves are characterized by the following dispersion relation:

$$\omega^2 = \frac{|u_0|^2 k^2}{1 + dk^2} + \frac{1}{4}k^4. \tag{16}$$

From the above equation we can obtain the following information. First, it is observed that $\omega \in \mathbb{R}\ \forall k \in \mathbb{R}$, which indicates that the steady-state solution is modulationally stable. This result is important since, below, we will seek for soliton solutions on top of the stable cw background (7). Second, in the long-wavelength limit, such that $dk^2 \ll 1$, Eq. (16) can be reduced to the following Bogoliubov-type dispersion relation:

$$\omega^2 \approx k^2 C^2 + \frac{1}{4}\alpha k^4, \tag{17}$$

where

$$C^2 = |u_0|^2, \tag{18}$$

is the squared "speed of sound", namely the velocity of linear waves propagating on top of the cw solution. In addition, parameter α is given by:

$$\alpha = 1 - 4d|u_0|^2, \tag{19}$$

and plays the role of an effective surface tension for our original system. Indeed, as discussed in Ref. [21], this can be inferred by the fact that Eq. (17) is reminiscent of the dispersion relation for shallow water waves [4]:

$$\omega^2 \approx k^2 c_0^2 + \frac{1}{3}\left(3\hat{T} - 1\right)c_0^2 h^2 k^4. \tag{20}$$

Here, $c_0^2 = gh$ is the velocity (g is the acceleration of gravity and h the depth of water at rest), while $\hat{T} = T/\left(\rho g h^2\right)$, where ρ is the density and T the surface tension. Comparing Eqs. (17) and (20), one can identify the correspondence: $3\hat{T} \to 4d|u_0|^2$, which indeed suggests that a *surface tension* analogue in our problem is $\propto d|u_0|^2$, depending on the nonlocality parameter d and the cw intensity $|u_0|^2$.

Obviously, regarding the magnitude of the effective surface tension, one may identify the following two regimes:

- $\alpha < 0 \Rightarrow 4d|u_0|^2 > 1$: weak surface tension – strong nonlocality (for fixed $|u_0|^2$),
- $\alpha > 0 \Rightarrow 4d|u_0|^2 < 1$: strong surface tension – weak nonlocality (for fixed $|u_0|^2$).

Below it will be shown that these two regimes correspond, respectively, to a KP-II and a KP-I equation, with the former giving rise to complex interactions of line solitons (that we will study in detail).

2.2 The nonlinear regime – asymptotic analysis

2.2.1 The intermediate stage – Bousinesq/Benney-Luke equation

We now proceed by analyzing the fully nonlinear regime. We start by seeking solutions of Eqs. (7)–(9) in the form of the following asymptotic expansions:

$$\rho = 1 + \varepsilon\rho_1 + \varepsilon^2\rho_2 + \cdots, \tag{21}$$

$$\phi = -|u_0|^2 t + \varepsilon^{1/2}\Phi \tag{22}$$

$$n = |u_0|^2 + \varepsilon n_1 + \varepsilon^2 n_2 + \cdots, \tag{23}$$

where $0 < \varepsilon \ll 1$ is a formal small parameter and the unknown functions ρ_j, Φ and n_j ($j = 1, 2, \ldots$) depend on the following stretched variables:

$$X = \varepsilon^{1/2}x, \quad Y = \varepsilon^{1/2}y, \quad T = \varepsilon^{1/2}t, \tag{24}$$

$$R = \varepsilon^{1/2}r, \quad \theta = \theta, \quad T = \varepsilon^{1/2}t, \tag{25}$$

for the Cartesian and polar geometry, respectively (the angular coordinate θ in the polar geometry remains unchanged). By substituting the expansions (21)–(23) into Eqs. (7)–(9), and equating terms of the same order in ε, we obtain the following results. First, Eq. (13), at $\mathcal{O}(\varepsilon^{3/2})$ and $\mathcal{O}(\varepsilon^{5/2})$, yields:

$$\rho_{1T} + \tilde{\Delta}\Phi = 0, \quad \rho_{2T} + \tilde{\nabla}\cdot\left(\rho_1\tilde{\nabla}\Phi\right) = 0. \tag{26}$$

Furthermore, Eq. (14) at $\mathcal{O}(\varepsilon)$ and $\mathcal{O}(\varepsilon^2)$ leads to the equations:

$$n_1 = |u_0|^2\rho_1, \quad d\tilde{\Delta}n_1 - n_2 + |u_0|^2\rho_2 = 0, \tag{27}$$

which connect the amplitudes $\rho_{1,2}$ and $n_{1,2}$ with the phase Φ; note that, here,

$$\tilde{\Delta} \equiv \partial_X^2 + \partial_Y^2, \quad \tilde{\nabla} \equiv (\partial_X, \partial_Y), \text{ or } \tilde{\Delta} \equiv \frac{1}{R}\partial_R(R\partial_R) + \frac{1}{R^2}\partial_\theta^2, \quad \tilde{\nabla} \equiv \left(\partial_R, \frac{1}{R}\partial_\theta\right), \tag{28}$$

in Cartesian and polar coordinates, respectively. In addition, Eq. (14) yields:

$$\Phi_T + n_1 + \varepsilon\left[\frac{1}{2}\partial_T\left(\tilde{\nabla}\Phi\right)^2 + n_2 - \frac{1}{4}\tilde{\Delta}\rho_1\right] = \mathcal{O}\left(\varepsilon^2\right). \tag{29}$$

To this end, combining Eq. (29) with Eqs. (26) and (27), yields the following biderectional nonlinear dispersive wave equation for Φ:

$$\Phi_{TT} - C^2\tilde{\Delta}\Phi + \varepsilon\left[\frac{1}{4}\alpha\tilde{\Delta}^2\Phi + \frac{1}{2}\partial_T\left(\tilde{\nabla}\Phi\right)^2 + \tilde{\nabla}\cdot\left(\Phi_T\tilde{\nabla}\Phi\right)\right] = \mathcal{O}\left(\varepsilon^2\right), \tag{30}$$

where C^2 is the squared speed of sound given by Eq. (18) and the parameter α is given by Eq. (19). Here it is worth observing the following. First, at the leading-order in ε, Eq. (30) is the standard second-order wave equation, while at order $\mathcal{O}(\varepsilon)$, the linear part of Eq. (30) corresponds to the dispersion relation (16) for the small-amplitude linear waves of Eqs. (2) and (3) propagating on top of the steady state with $|u| = |u_0|$ and $n = |u_0|^2$. The full Eq. (30), incorporates fourth-order dispersion and quadratic nonlinear terms, resembling the Boussinesq and Benney-Luke [24] equations. These models, are used to describe bidirectional shallow water waves, in the framework of small-amplitude and long-wave approximations [4].

2.2.2 Long-time behavior – KP equation

Using a multiscale expansion method, similar to the one employed in the water wave problem [4], we now derive the KP equation, which is obtained under the additional assumptions of *quasi-two-dimensionality* and *unidirectional propagation*. In particular, we introduce the asymptotic expansion:

$$\Phi = \Phi_0 + \varepsilon\,\Phi_1 + \cdots, \tag{31}$$

where the unknown functions Φ_ℓ ($\ell = 0, 1, \ldots$) depend on the variables:

$$\chi = X - CT, \quad \tilde{\chi} = X + CT, \quad \mathcal{Y} = \varepsilon^{1/2}Y, \quad \mathcal{T} = \varepsilon T, \tag{32}$$

$$\varrho = R - CT, \quad \tilde{\varrho} = R + CT, \quad \Theta = \varepsilon^{-1/2}\theta, \quad \mathcal{T} = \varepsilon T, \tag{33}$$

for the Cartesian and polar geometry, respectively. Substituting the expansion (31) into Eq. (30), at the leading-order in ε, we obtain the equations:

$$\Phi_{0\chi\tilde{\chi}} = 0, \tag{34}$$

$$\Phi_{0\varrho\tilde{\varrho}} = 0, \tag{35}$$

in Cartesian and polar coordinates respectively. The above equations imply that Φ_0 can be expressed as a superposition of two waves. In the Cartesian geometry, these waves are a right-going one, $\Phi_0^{(R)}$, which depends on χ, and a left-going one, $\Phi_0^{(L)}$, depending on $\tilde{\chi}$. Similarly, in the polar case, Φ_0 can be expressed as superposition of a radially expanding wave (depending on ϱ), and a radially contracting one (depending on $\tilde{\varrho}$). Thus, the solutions of Eqs. (34) and (35) read:

$$\Phi_0 = \Phi_0^{(R)}(\chi, \mathcal{Y}, \mathcal{T}) + \Phi_0^{(L)}(\tilde{\chi}, \mathcal{Y}, \mathcal{T}), \tag{36}$$

$$\Phi_0 = \Phi_0^{(R)}(\varrho, \Theta, \mathcal{T}) + \Phi_0^{(L)}(\tilde{\varrho}, \Theta, \mathcal{T}). \tag{37}$$

In addition, at order $\mathcal{O}(\varepsilon)$, we obtain the following equations:

$$\begin{aligned} 4C^2\Phi_{1\chi\tilde{\chi}} = & -C\left(\Phi_{0\chi\chi}^{(R)}\Phi_{0\tilde{\chi}}^{(L)} - \Phi_{0\chi}^{(R)}\Phi_{0\tilde{\chi}\tilde{\chi}}^{(L)}\right) \\ & + \left[\partial_\chi\left(-2C\Phi_{0\mathcal{T}}^{(R)} + \frac{\alpha}{4}\Phi_{0\chi\chi\chi}^{(R)} - \frac{3C}{2}\Phi_{0\chi}^{(R)2}\right) - C^2\Phi_{0\mathcal{Y}\mathcal{Y}}^{(R)}\right] \\ & + \left[\partial_{\tilde{\chi}}\left(2C\Phi_{0\mathcal{T}}^{(L)} + \frac{\alpha}{4}\Phi_{0\tilde{\chi}\tilde{\chi}\tilde{\chi}}^{(L)} + \frac{3C}{2}\Phi_{0\tilde{\chi}}^{(L)2}\right) - C^2\Phi_{0\mathcal{Y}\mathcal{Y}}^{(L)}\right], \end{aligned} \tag{38}$$

for the Cartesian geometry, and

$$\begin{aligned} 4C^2\Phi_{1\varrho\tilde{\varrho}} = & -C\left(\Phi_{0\varrho\varrho}^{(R)}\Phi_{0\tilde{\varrho}}^{(L)} - \Phi_{0\varrho}^{(R)}\Phi_{0\tilde{\varrho}\tilde{\varrho}}^{(L)}\right) \\ & + \left[\partial_\rho\left(-2C\Phi_{0\mathcal{T}}^{(R)} + \frac{\alpha}{4}\Phi_{0\varrho\varrho\varrho}^{(R)} - \frac{3C}{2}\Phi_{0\varrho}^{(R)2} - \frac{C}{\mathcal{T}}\Phi_{0\tilde{\varrho}}^{(R)}\right) - \frac{1}{\mathcal{T}^2}\Phi_{0\Theta\Theta}^{(R)}\right] \\ & + \left[\partial_{\tilde{\varrho}}\left(2C\Phi_{0\mathcal{T}}^{(L)} + \frac{\alpha}{4}\Phi_{0\tilde{\varrho}\tilde{\varrho}\tilde{\varrho}}^{(L)} + \frac{3C}{2}\Phi_{0\tilde{\varrho}}^{(L)2} - \frac{C}{\mathcal{T}}\Phi_{0\tilde{\varrho}}^{(L)}\right) - \frac{1}{\mathcal{T}^2}\Phi_{0\Theta\Theta}^{(R)}\right], \end{aligned} \tag{39}$$

for the polar geometry. Here, it is important to observe the following. Once Eq. (38) is integrated in χ or $\tilde{\chi}$ [and, similarly, Eq. (39) in ϱ or $\tilde{\varrho}$], secular terms arise: the secular therms are those in the square brackets in the right-hand side, because are functions of χ or $\tilde{\chi}$ (ϱ or $\tilde{\varrho}$ in polar) alone, not both. Removal of these secular terms leads to two uncoupled nonlinear evolution equations for $\Phi_0^{(R)}$ and $\Phi_0^{(L)}$ in both geometries. Furthermore, using the equation $\Phi_T = -n_1$ (i.e., the linear part of Eq. (29), together with Eqs. (26) and (27), it is found that the amplitude ρ_1 can also be decomposed to a left- and a right-going wave; this means that

$$\rho_1 = \rho_1^{(R)} + \rho_1^{(L)},$$

with the fields $\rho_1^{(R)}$ and $\rho_1^{(L)}$ satisfying a pair of two uncoupled KP equations. In the Cartesian geometry, the KP equations are of the form:

$$\partial_\chi\left(\rho_{1\mathcal{T}}^{(R)} - \frac{\alpha}{8C}\rho_{1\chi\chi\chi}^{(R)} + \frac{3C}{2}\rho_1^{(R)}\rho_{1\chi}^{(R)}\right) + \frac{C}{2}\rho_{1\mathcal{Y}\mathcal{Y}}^{(R)} = 0, \tag{40}$$

$$\partial_{\tilde{\chi}}\left(\rho_{1\mathcal{T}}^{(L)} + \frac{\alpha}{8C}\rho_{1\tilde{\chi}\tilde{\chi}\tilde{\chi}}^{(L)} - \frac{3C}{2}\rho_1^{(L)}\rho_{1\tilde{\chi}}^{(L)}\right) - \frac{C}{2}\rho_{1\mathcal{Y}\mathcal{Y}}^{(L)} = 0, \tag{41}$$

while in the polar geometry, the relevant equations take the form of the so-called cylindrical KP (cKP), or Johnson's equations (see Refs. [22, 23]):

$$\partial_\varrho\left(\rho_{1\mathcal{T}}^{(R)}-\frac{\alpha}{8C}\rho_{1\varrho\varrho\varrho}^{(R)}+\frac{3C}{2}\rho_1^{(R)}\rho_{1\chi}^{(R)}+\frac{1}{2\mathcal{T}}\rho_1^{(R)}\right)+\frac{1}{2C\mathcal{T}^2}\rho_{1\Theta\Theta}^{(R)}=0, \tag{42}$$

$$\partial_{\tilde{\varrho}}\left(\rho_{1\mathcal{T}}^{(L)}+\frac{\alpha}{8C}\rho_{1\tilde{\varrho}\tilde{\varrho}\tilde{\varrho}}^{(L)}-\frac{3C}{2}\rho_1^{(L)}\rho_{1\tilde{\varrho}}^{(L)}-\frac{1}{2\mathcal{T}}\rho_1^{(L)}\right)-\frac{1}{2C\mathcal{T}^2}\rho_{1\Theta\Theta}^{(L)}=0. \tag{43}$$

2.2.3 Versions of the KP equations

It is now convenient to further simplify the equations above, namely the KP and the cKP equations, in order to express them in their standard form [4]. We consider right-going waves in the Cartesian geometry, and radially expanding ones in the polar geometry, and introduce the following transformations,

$$\mathcal{Y}\mapsto\sqrt{\frac{3|\alpha|}{4C^2}}\mathcal{Y},\quad \Theta\to\sqrt{\frac{3|\alpha|}{4}}\Theta,\quad \mathcal{T}\mapsto-\frac{\alpha}{8C}\mathcal{T},\quad \rho_1^{(R)}=-\frac{\alpha}{2C^2}U, \tag{44}$$

which cast the respective KP and cKP equations into the following form:

$$\partial_\mathcal{X}(U_\mathcal{T}+6UU_\mathcal{X}+U_{\mathcal{X}\mathcal{X}\mathcal{X}})+3\sigma^2U_{\mathcal{Y}\mathcal{Y}}=0, \tag{45}$$

$$\partial_\varrho\left(U_\mathcal{T}+6UU_\varrho+U_{\varrho\varrho\varrho}+\frac{1}{2\mathcal{T}}U\right)+\frac{3\sigma^2}{\mathcal{T}^2}U_{\Theta\Theta}=0. \tag{46}$$

Here, the parameter σ^2 is defined as:

$$\sigma^2=-\operatorname{sgn}\alpha=\operatorname{sgn}\left(4d|u_0|^2-1\right). \tag{47}$$

It is now clear that, in the Cartesian case, Eq. (45) includes both versions of the KP equation, KPI and KPII [33]. Indeed, for $\sigma^2=1\Rightarrow\alpha<0$, i.e., for $|u_0|^2>1/(4d)$ or $d>1/(4|u_0|)^2$, Eq. (45) is a KPII equation; this corresponds to a small effective surface tension. On the other hand, for $\sigma^2=-1\Rightarrow\alpha>0$, i.e., $|u_0|^2<1/(4d)$ or $d<1/(4|u_0|)^2$, Eq. (45) is a KPI equation; this corresponds to the case of large effective surface tension (see end of Section 2.1 and discussion below).

In other words, for a fixed degree of nonlocality d, a larger (smaller) background amplitude $|u_0|$, as defined by the sign of α, corresponds to KPII (KPI); similarly, for a fixed background amplitude $|u_0|$, a strong (weak) nonlocality, as defined by the above regimes of d, corresponds to KPII (KPI). Notice that in the local limit of $d=0$, the asymptotic analysis leads only to the KPI model, in which line solitons are unstable; this fact was used to better understand self-focusing and transverse instability of plane dark solitons of the defocusing NLS Equation [19, 20]. Notably, the same parameter α can also been shown to distinguish solutions in 1D [34] and radially symmetric [35] systems; a similar case, pertinent to the polar geometry, will be considered below.

Once again, it is important to highlight the fact that the existence of these regimes resembles the situation occurring in shallow water. In this context, weak surface tension corresponds to $\sigma^2=1$ in Eq. (45) (i.e., KPII), while strong surface tension is pertinent to $\sigma^2=-1$ (i.e., KPI). Thus, there exists an immediate connection between the original problem with the one of shallow water waves: relatively

large (small) background amplitude or nonlocality corresponds to weak (strong) surface tension, leading to KPII (KPI).

3. Approximate soliton solutions

We now employ the results of the above analysis and construct the solution of our original problem. This can be done as follows. Once a solution of Eq. (45) [or (46)] is known, an approximate solution of Eqs. (2) and (3) has the form:

$$u \approx u_0 \left(1 - \varepsilon \frac{\alpha}{2|u_0|^2} U\right)^{1/2} \exp\left(-i|u_0|^2 t + \frac{i}{2}\alpha\varepsilon^{-1/2}\int_0^{\mathcal{T}} U d\mathcal{T}'\right), \tag{48}$$

$$n \approx |u_0|^2 - \frac{1}{2}\varepsilon\alpha U. \tag{49}$$

It is important to note that Eq. (48) describes two different types of solitons, namely dark and antidark ones. Indeed, for $\alpha < 0$, i.e., for solutions satisfying the KPII equation (corresponding to the *strong nonlocality regime*) the solution (48) has the form of a *hump* on top of the cw background and is, thus, an *antidark soliton*. On the other hand, for $\alpha > 0$, i.e., for solutions satisfying the KPI equation (corresponding to the *weak nonlocality regime*) the solution (48) has the form of a *dip* on top of the cw background and is, thus, a *dark soliton*. Note that in the local limit, with $d = 0$, it turns out that $\alpha = 1$ and the solutions have always the form of dark solitons. In other words, antidark solitons are only supported by a sufficiently strong nonlocality.

Below, we will use known solutions of the KP and cKP equations and present corresponding solutions of the nonlocal NLS. In addition, we will perform direct numerical simulations to examine the evolution and – in some cases – the interaction dynamics of the approximate soliton solutions (48).

3.1 Antidark stripe solitons and their interactions

We start with the Cartesian geometry and consider, in particular, the simplest soliton solutions of the KP equation, the so-called line solitons. Specifically, the one-line soliton solution of Eq. (45), traveling at an angle to the Y-axis, reads [33]:

$$\begin{aligned} U(\mathcal{X}, \mathcal{Y}, \mathcal{T}) &= 2\kappa^2 \mathrm{sech}^2(Z), \\ Z &\equiv \kappa\left[\mathcal{X} + \lambda\mathcal{Y} - \left(\kappa^2 + 3\lambda^2\right)\mathcal{T} + \delta\right], \end{aligned} \tag{50}$$

where κ, λ and δ are free parameters. We are particularly interested in the case where the corresponding solution of the NLS takes the form of an antidark soliton, with U obeying the KPII equation: since, in this case, line solitons are stable, we may expect that their interactions will give rise to patterns resembling those observed in shallow water [5]. An example of such an antidark soliton is ahown in **Figure 1**, for $t = 0$. For this example, the following parameter values were used: $u_0 = 1$ and $d = 1/\sqrt{3}$ (leading to $\alpha = -1/3 < 0$), as well as $\kappa = \lambda = 1$, $\delta = 0$, and $\varepsilon = 0.2$. These values will also be used below.

In what follows, we choose line solitons with specific parameters, so that their angle during interaction will determine the type of pattern. In the simulations, we evolve the initial configuration up to $t = 600$, so that solitons have enough time to interact and generate interesting interaction patterns. In all cases, the numerical integration of Eqs. (2) and (3) is performed via a high-accuracy pseudo-spectral

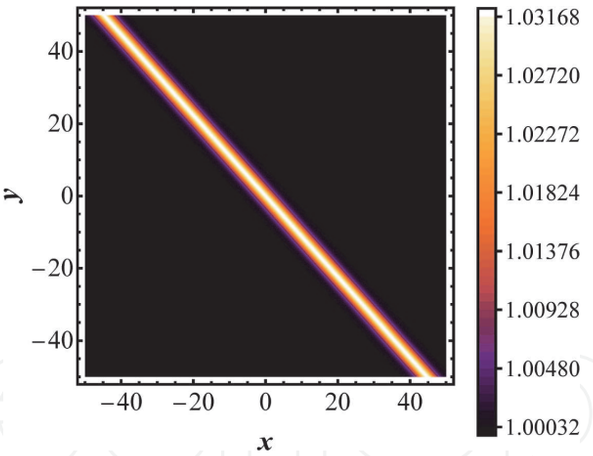

Figure 1.
A typical single antidark soliton solution of the nonlocal NLS ($u(x,y,0)$), with $\kappa = \lambda = 1$, $\delta = 0$; other parameter values are: $u_0 = C = 1$, $d = 1/\sqrt{3}$, and $\varepsilon = 0.2$.

method in space and fourth-order in time. To adjust to the periodic boundary conditions, the scheme requires we place the solutions on top of a wide super-Gaussian background that decays at infinity and makes the initial condition periodic. As it will be seen below, interacting antidark NLS solitons follow closely the KP dynamics, giving rise to patterns that are usually observed in water.

We start with the interaction of two solitons, and express the two-line soliton solution of KPII as follows:

$$\begin{gathered} U(\mathcal{X},\mathcal{Y},\mathcal{T}) = 2\partial_{\mathcal{X}}^2 \ln F(\mathcal{X},\mathcal{Y},\mathcal{T}), \\ F \equiv 1 + \exp(Z_1) + \exp(Z_2) + \exp(Z_1 + Z_2 + A_{12}), \\ \exp(A_{12}) = \frac{(\kappa_1 - \kappa_2)^2 - (\lambda_1 - \lambda_2)^2}{(\kappa_1 + \kappa_2)^2 - (\lambda_1 - \lambda_2)^2}, \end{gathered} \tag{51}$$

with $Z_i \equiv \kappa_i\left[\mathcal{X} + \lambda_i\mathcal{Y} - \left(\kappa_i^2 + 3\lambda_i^2\right)\mathcal{T} + \delta_i\right]$.

We first focus on interacting line solitons that form Y- and X-shaped waveforms, and proceed with more complex ones later in the text. In **Figure 2**, we show a typical Y-shaped pattern, whereby the resonant two-soliton interaction gives rise to the emergence of one soliton, with its maximum height being four times that of the incoming solitons (this resonant Y-shaped solution was originally found by

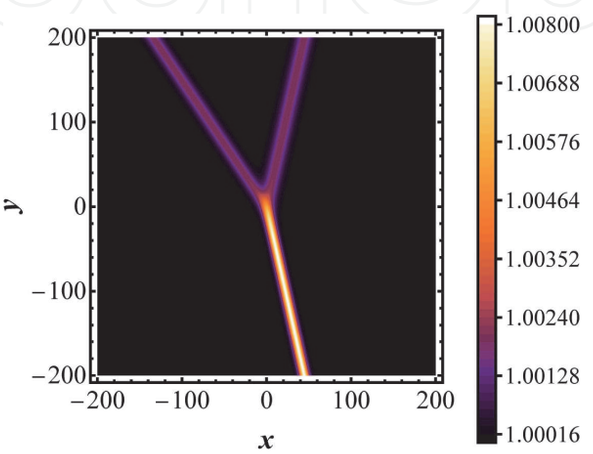

Figure 2.
A typical Y-type interaction, $u(x,y,0)$, whereby out of two incoming colliding solitons, a single line soliton emerges. Parameter values are: $\kappa_1 = \kappa_2/2 = 1/2$, $\lambda_1 = 3\lambda_2 = 3/4$.

Miles [7, 8]). This feature is clearly observed in the figure. Parameter values in this case are: $\kappa_1 = \kappa_2/2 = 1/2$, $\lambda_1 = 3\lambda_2 = 3/4$ (and for all cases, also pertaining to X-type interactions below, $\delta_1 = \delta_2 = 0$).

Next, we proceed with the X-type interactions, which can be discriminated according to the resulting "stem": an interaction with a *short stem* (**Figure 3**-left), an interaction with a long stem where the stem height is higher than the incoming line solitons (**Figure 3**-middle and right respectively).

In the same category falls an X-type interaction with a long stem, with the stem height being lower than the tallest incoming line soliton, which we refer to here as an H-interaction. A typical such interaction is given in **Figure 4**, and parameter values: $\kappa_1 = \kappa_2/2 = 1/2$, $\lambda_1 = 1/2 - 10^{-7}$, and $\lambda_2 = 0$.

An immediate generalization of the above is a three-wave interaction, where now

$$F = 1 + \sum_{1 \le i \le 3} e^{\eta_i} + \sum_{1 \le i < j \le 3} e^{\eta_i + \eta_j + A_{ij}} + e^{\eta_1 + \eta_2 + \eta_3 + A_{12} + A_{13} + A_{23}}, \tag{52}$$

and

$$\exp\left(A_{ij}\right) = \frac{\left(\kappa_i - \kappa_j\right)^2 - \left(\lambda_i - \lambda_j\right)^2}{\left(\kappa_i + \kappa_j\right)^2 - \left(\lambda_i - \lambda_j\right)^2}, \tag{53}$$

so that the resulting interaction is as in **Figure 5**, for $t = 200$. Here, $\kappa_1 = 1$, $\kappa_2 = 2$, $\kappa_3 = 3$, $\lambda_1 = \lambda_2/2 = \lambda_3/5 = -1/3$ and, as before, $\delta_1 = \delta_2 = \delta_3 = 0$.

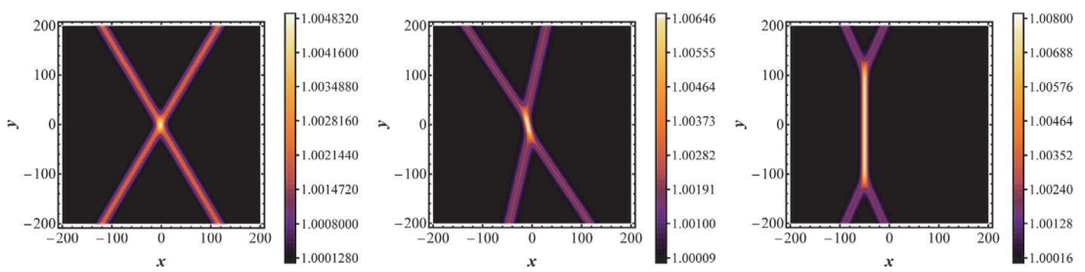

Figure 3.
X-type interactions, $u(x, y, 0)$, with: $\kappa_1 = \kappa_2 = 1/2$, $\lambda_1 = -\lambda_2 = -2/3$ (left), $\kappa_1 = \kappa_2 = 1/2$, $\lambda_1 = 1/4 - 0.01$, $\lambda_2 = 3/4$ (middle), $\kappa_1 = \kappa_2 = 1/2$, $\lambda_1 = 1/2$, $\lambda_2 = -1/2 - 10^{-10}$ (right). Observe that the length of the stem is increased from left to right (see also text).

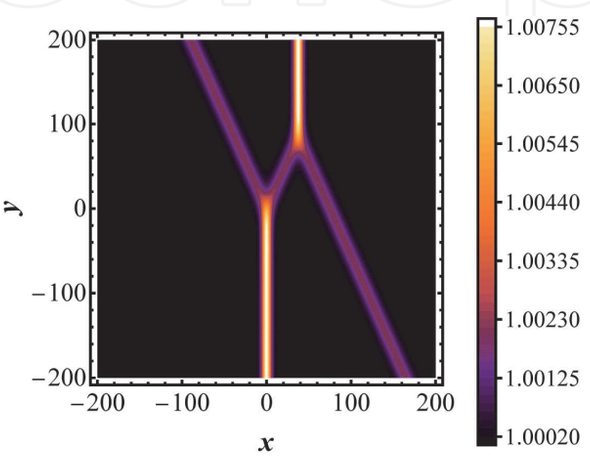

Figure 4.
An H-type interaction, $u(x, y, 0)$, with $\kappa_1 = \kappa_2/2 = 1/2$, $\lambda_1 = 1/2 - 10^{-7}$, $\lambda_2 = 0$.

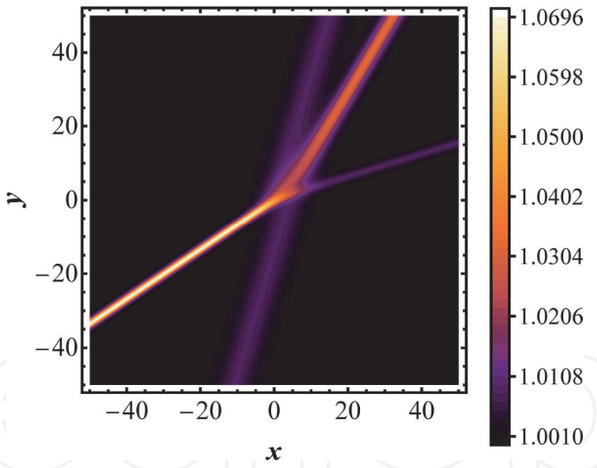

Figure 5.
A 2–3 wave interaction, $u(x,y,0)$, with $\kappa_1 = 1$, $\kappa_2 = 2$, $\kappa_3 = 3$, $\lambda_1 = \lambda_2/2 = \lambda_3/5 = -1/3$ and $\delta_1 = \delta_2 = \delta_3 = 0$.

More intricate structures may still form whose mathematical description is more complex. Such novel weblike structures for the KP equation, termed N-in M-out, have been found using Wronskian methods [11, 13, 15] and the so-called τ-function. We illustrate the basic construction of these solitons but do not go into further detail as this is beyond the scope of this work. The most convenient way to write the line soliton solutions of the KPII system is through the Wronskian, or τ-function, which replaces the F function above. Now, the solutions of the KPII equation are written in a similar manner as above, as

$$U(\mathcal{X},\mathcal{Y},\mathcal{T}) = 2\partial_{\mathcal{X}}^2 \ln \tau(\mathcal{X},\mathcal{Y},\mathcal{T}), \tag{54}$$

where this new τ-function represents the Wronskian determinant

$$\tau(\mathcal{X},\mathcal{Y},\mathcal{T}) = \begin{pmatrix} f_1 & f_2 & \cdots & f_N \\ f_1' & f_2' & \cdots & f_N' \\ \vdots & \vdots & \cdots & \vdots \\ f_1^{(N-1)} & f_2^{(N-1)} & \cdots & f_N^{(N-1)} \end{pmatrix}. \tag{55}$$

Here superscripts denote differentiation with respect to X, and the set of f_n functions constitute the set of linearly independent solutions of the system:

$$f_{\mathcal{Y}} = f_{\mathcal{X}\mathcal{X}}, \quad f_{\mathcal{T}} = f_{\mathcal{X}\mathcal{X}\mathcal{X}}. \tag{56}$$

In particular, for line solitons these are defined as:

$$f_n(\mathcal{X},\mathcal{Y},\mathcal{T}) = \sum_{m=1}^{M} a_{nm} e^{\theta_m}, \;\; n = 1,2,\ldots,N, \tag{57}$$

where $\theta_m = k_m\mathcal{X} + k_m^2\mathcal{Y} + k_m^3\mathcal{T} + \theta_{0m}$ with distinct real parameters k_m 's with the property: $k_1 < k_2 < \cdots < k_M$. The parameters θ_{0m} are real constants. Importantly, the coefficients a_{nm} define an $N \times M$ matrix of rank N, due to the linear independence of the functions f_n, such that $(a_{nm} =: A)$. Below we provide two examples, and their evolution for a 2–2 and 3–3 interaction (see **Figures 6** and **7**, respectively).

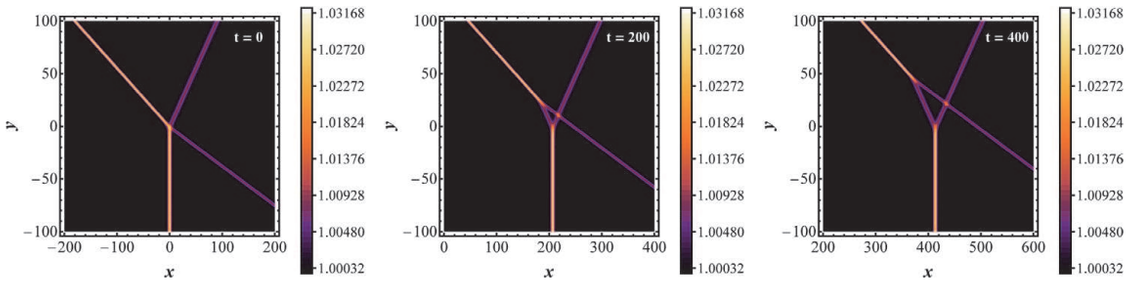

Figure 6.
A typical 2–2 wave evolution for $t = 0$ (left), $t = 200$ (middle) and $t = 400$ (right). All figures refer to the variable $u(x, y, t)$.

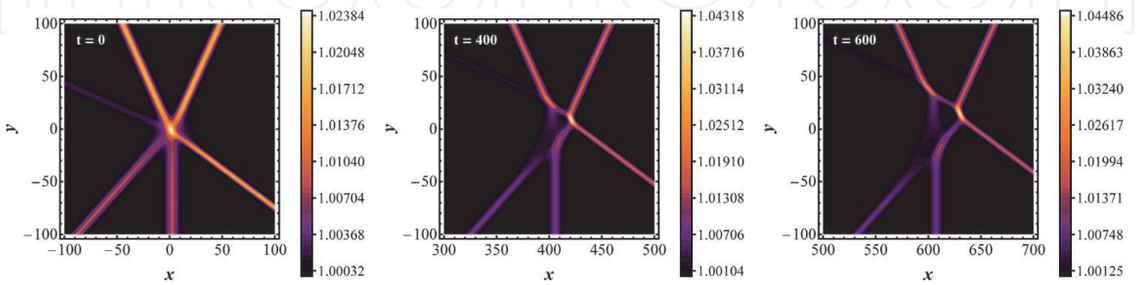

Figure 7.
A typical 3–3 wave evolution, for $t = 0$ (left), $t = 400$ (middle), and $t = 600$ (right). All figures refer to the variable $u(x, y, t)$.

We start with a 2–2 interaction, by defining the matrix A, such that

$$A = \begin{pmatrix} 1 & 0 & -1 & -1 \\ 0 & 1 & 1 & 1 \end{pmatrix}, \tag{58}$$

and the relative real parameters $k_1 = -1$, $k_2 = 0$, $k_3 = 1$ and $k_4 = 2$ corresponding to the relative $\theta_m|_{m=1}^4$. Then, the evolution of this interaction is depicted in **Figure 6**.

Similarly, for a 3–3 wave interaction one has:

$$A = \begin{pmatrix} 1 & 0 & -1 & -1 & 0 & 2 \\ 0 & 1 & 2 & 1 & 0 & -1 \\ 0 & 0 & 0 & 0 & 1 & 1 \end{pmatrix}, \tag{59}$$

and $k_1 = -1$, $k_2 = -1/2$, $k_3 = 0$, $k_4 = 1/2$, $k_5 = 1$ and $k_6 = 3/2$ to produce the following interaction pattern of **Figure 7**.

It is important to note here that the matrices A for the 2–2 and 3–3 solitons, are not arbitrarily chosen. The $N \times N$ maximal minors of A must be non-negative in order for the KP solution q to be regular for all X, Y and T. In the literature, such matrices are called totally non-negative matrices.

3.2 Dark lump solitons

So far, we have focused on structures obeying the effective KPII equation. These structures, namely the antidark stripe solitons, are quasi one-dimensional (1D) states, which are stable. The respective states that satisfy the effective KPI equation, namely dark stripe solitons, are expected to be transversely unstable – see, e.g., Ref. [36] for a stability analysis of KP line solitons.

Nevertheless, the KPI equation, that corresponds to the weakly nonlocal regime, supports stable, purely 2D, soliton states known as *lumps*. These solitons are weakly localized, namely they decay algebraically as $|x|, |y| \to \infty$. The respective solitons of the nonlocal NLS, which are of the dark type, i.e., they have the form of dark lumps, can be effectively described as solutions of Eq. (45) for the field U:

$$U(\mathcal{X},\mathcal{Y},\mathcal{T}) = 16\frac{16q^2\eta^2 - 4(\xi - 2k\eta)^2 + 1/q^2}{\left[16q^2\eta^2 + 4(\xi - 2k\eta)^2 + 1/q^2\right]^2}, \qquad (60)$$
$$\xi = \mathcal{X} - 12\left(k^2 + q^2\right)\mathcal{T}, \quad \eta = \mathcal{Y} - 12k\mathcal{T},$$

where q and k are free real parameters. Notice that solutions of this type have not yet been observed in water due to the fact that the surface tension is small.

Similarly to the case of antidark stripe solitons, once Eq. (60) is substituted into Eq. (48) gives rise to the approximate dark lump soliton of the nonlocal NLS. Using the relevant analytical expression, it is straightforward to prepare the corresponding initial condition by setting $t = 0$, and numerically integrate Eqs. (2) and (3) to examine the evolution of dark lumps. In **Figure 8**, shown is the result of such a simulation for the dark lump; for this simulation, we have used the parameter values $u_0 = 1$, $d = 1/5$ (so that $\alpha = 1/5 > 0$, corresponding to dark soliton states), as well as $k = 0$ and $q = 1$. It can readily be observed that the dark lump solitons propagate undistorted up to $t = 20$, which is the "numerical horizon" for this particular simulation. This result indicates that, similarly to antidark stripe solitons, dark lumps can also be supported by the nonlocal NLS system.

3.3 Ring dark and antidark solitons

We now turn our attention to the cKP Eq. (46), and focus on radially symmetric solutions that do not depend on Θ. In such a case, Eq. (46) reduces to a quasi-1D equation, namely the cylindrical Korteweg-de Vries (cKdV), which is also a

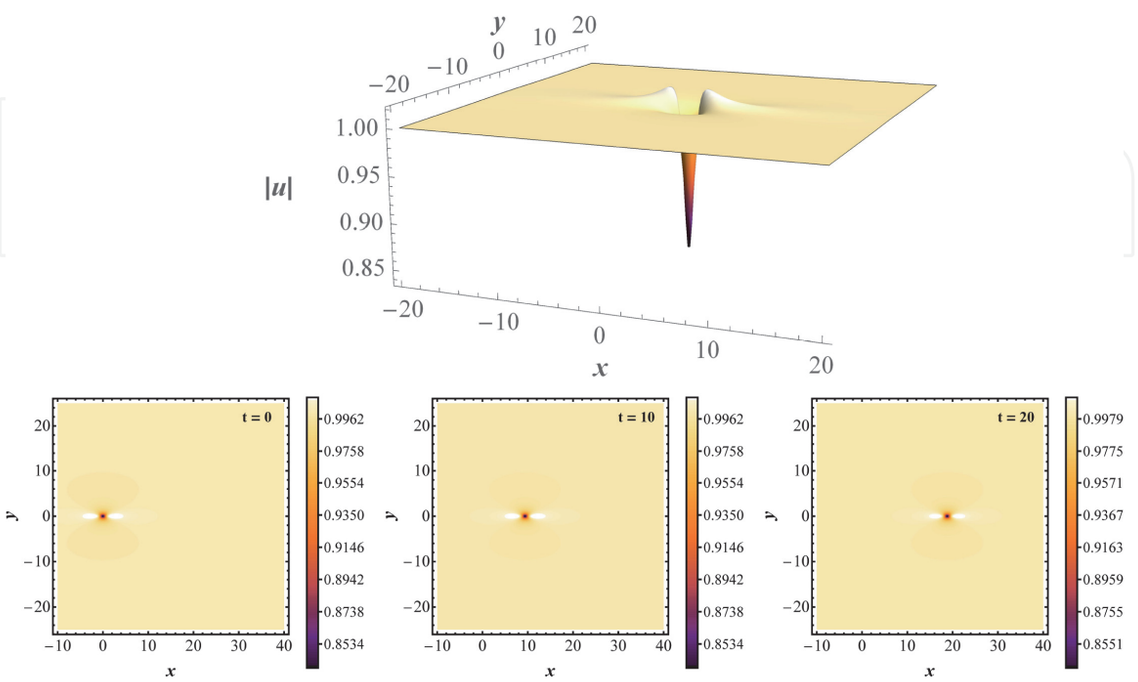

Figure 8.
A typical dark lump solution, at $t = 0$, with $k = 0$, $q = 1$ (top panel) and its evolution for $t = 0$, 10 and 20. The initial condition shown in the top panel is given by Eq. (60).

completely integrable model. The cKdV is a generic equation that can been used to describe cylindrical solitons in shallow water, plasmas, etc. [1]. As was shown in Ref. [37], the cKdV equation admits an exact soliton solution which, in the framework of Eq. (46), can be expressed as follows:

$$U(\varrho,\mathcal{T}) = \frac{\varrho}{12\mathcal{T}} + \frac{2\kappa^2}{\mathcal{T}}\,\mathrm{sech}^2\left(\frac{8\kappa^3}{\sqrt{\mathcal{T}}} + \frac{\kappa\varrho}{\sqrt{\mathcal{T}}} + \varrho_0\right) \tag{61}$$

where η and ϱ_0 are free parameters of the soliton. It is clear that Eq. (61) has the form of a sech^2-pulse on top of a rational background. A clearer picture regarding the structure of the cKdV equation, can be obtained by means of an asymptotic asymptotic analysis [38, 39]. Indeed, as shown in these works, to leading-order, in the regime $|\mathcal{T}| \gg |\varrho|$, the primary wave $U(\varrho,\mathcal{T})$, decays to zero at both upstream and downstream infinity. The primary wave has a form similar to that of Eq. (50), but with the following change of variables: $\mathcal{X} \mapsto \varrho$ and $\delta \mapsto \varrho_0$. However, there is a very important difference: κ now becomes a slowly-varying function of $\mathcal{T}$, due to the presence of the term $U/(2\mathcal{T})$ in the cKdV. Following the analysis of [38, 39], and using the original coordinates, it can be concluded that:

$$\kappa^2 = \kappa_0^2\left(\frac{t_0}{t}\right)^{2/3}, \tag{62}$$

where κ_0^2 is a constant setting the solitary wave amplitude at $t = t_0$. We can know express an approximate solution of Eqs. (2) and (3), for the polar chase, and for the primary solitary wave. This is of the form of Eq. (48), with the soliton amplitude and velocity varying as $t^{-2/3}$, and the width varying as $t^{1/3}$, as follows from Eqs. (50) and (62).

Notice that this approximate solution is a ring-shaped solitary wave, on top of cw background, which can be either dark (for $\alpha > 0$) or anti-dark (for $\alpha < 0$). Notice, also that ring dark solitons were predicted to occur in optical media exhibiting either Kerr [40] or non-Kerr [41] nonlinearities, and were later observed in experiments [42]. On the other hand, ring anti-dark solitons were only predicted to occur in non-Kerr – e.g., saturable media [41, 43]. This picture is complemented by this analysis, according to which a relatively strong [i.e., $d > (1/4|u_0|)^2$] nonlocal nonlinearity can also support ring anti-dark solitary waves.

As in the Cartesian case, we have performed direct numerical simulations to examine the evolution of ring-shaped solitons in the nonlocal NLS model. First, in **Figure 9**, shown are 3D plots depicting the profiles of the ring dark solitons and ring antidark solitons. Here, we use $d = 1/5$ for the dark soliton ($\alpha > 0$) and $d = 1/3$ for

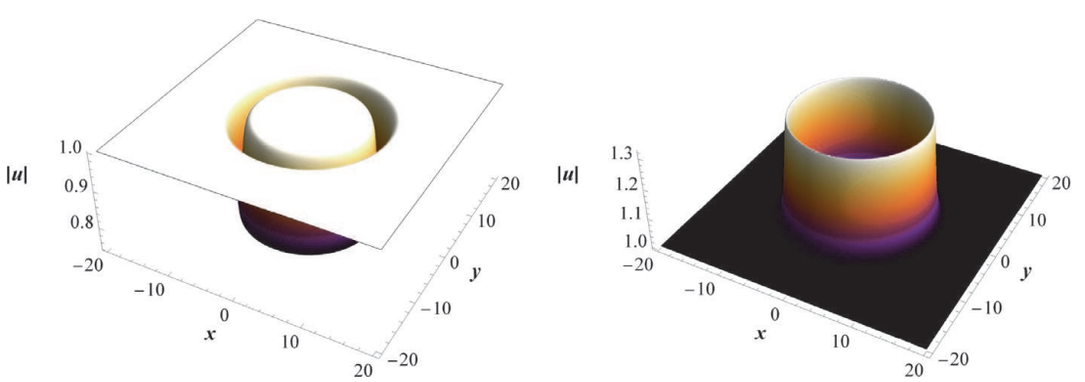

Figure 9.
(Color online) typical ring dark (left) and anti-dark (right) solitons.

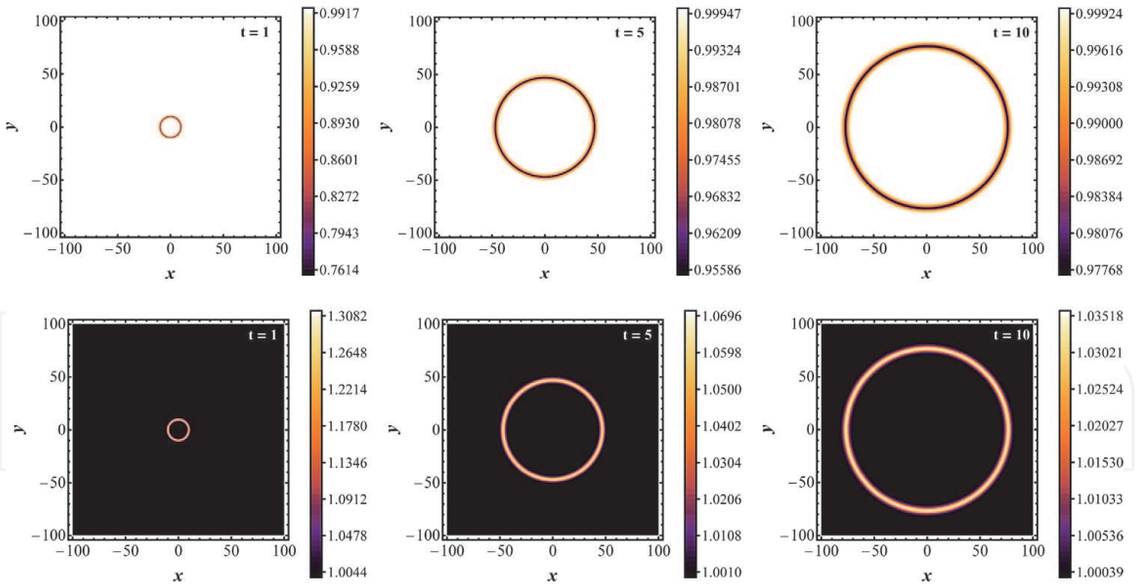

Figure 10.
(Color online) the evolution of the dark (top) and anti-dark (bottom) ring solitons of ***Figure 9****.*

the antidark ($\alpha < 0$), while the rest of the parameters are set equal to unity except $\varepsilon = 0.2$ as before. Furthermore, both solitons have an initial radius of $r(0) = 10$.

In addition, in **Figure 10**, we show the evolution of the ring solitons depicted in **Figure 9**. Once again, it is observed, that both types of ring solitons propagate undistorted up to end of the simulation ($t = 10$), which indicates that these states are also supported by the nonlocal NLS.

4. Conclusions and discussion

In conclusion, we have studied a 2D defocusing NLS model with a spatially nonlocal nonlinearity. The considered model is relevant to optical beam propagation in a variety of physical settings, including thermal media, plasmas, and nematic liquid crystals. We have analytically treated this nonlocal NLS by means of a two-stage multiscale analysis. This led to a Boussinesq/Benney-Luke-type equation, and a KP equation (in both Cartesian and polar geometries), which are models arising in the context of shallow water waves. This analysis revealed that the nonlocal NLS is characterized by an *effective surface tension*, which is related to the degree of nonlocality: small (large) effective surface tension corresponds to the strong (weak) nonlocality regime, whereby the asymptotic reduction leads to a KPII (KPI) equation.

Apart from the type of KP (KPII or KPI), the effective surface tension also controls the type of soliton: antidark (dark) solitons on top (off) the cw pedestal can only be formed in the strong (weak) nonlocality regime. We have thus found a number of different soliton states that can be supported by the nonlocal NLS. These include antidark stripe solitons, dark lump solitons, as well as ring dark and antidark solitons (in the polar case). We also used numerical simulations to examine the existence, evolution, as well as interaction dynamics. For the latter, we focused on the case of antidark solitons, which were shown to form a plethora of patterns coming out of their collisions. These include Y-, X-, H-shaped waveforms, as well as more complicated patterns involving more than two solitons; all these, have been observed in shallow water [5], a fact that highlights the deeper connection between water waves and light! In addition, we examined, by means of direct simulations, the existence and propagation of other soliton states, namely dark lump solitons, as

well as ring dark and antidark solitons. We found that all these states do exist in the framework of the nonlocal NLS, and can propagate undistorted up to times set by the simulations.

At this point, it is also relevant to comment on the possibility of observing the predicted patterns in real experiments. In that regard, first we consider the case of antidark solitons. The observation of these states took place some time ago, as it was first reported in Ref. [44]; this fact indicates that the necessary experimental setting is already available. As concerns the experimental set up needed for the observation of the Y-, X- and H-waves and other related patterns, it may be similar to that of Ref. [44]. In particular, one may employ at first a cw laser beam, which is split into two parts via a beam-splitter. One branch goes through a cavity system to form a pulse (as happens in typical pulsed lasers); this pulse branch undergoes phase-engineering, i.e., passes through a phase mask so that the characteristic phase jump of the antidark soliton is inscribed. Then, the cw and the phase-engineered pulse are incoherently coupled inside the nonlocal medium, e.g., a nematic liquid crystal. This process forms one antidark soliton, as in Ref. [44]. To observe the Y-, X- or H-patterns predicted above, two such antidark solitons have to be combined inside the crystal. The angle between the two incident beams, which should be appropriately chosen so that a specific pattern be formed, can be controlled by a rotating mirror in one of the branches of the beam-splitter.

As concerns the possibility of the experimental observation of the other soliton states that were predicted by our analysis, we note the following. First, regarding the weakly localized dark lump solitons, they can be experimentally observed as follows. In a real experiment, it is straightforward to create a dark soliton by using, e.g., a proper phase mask (see, e.g., the review [45] and references therein); this can also be done even in the case of *ring dark solitons* [46]. Such structures are prone to the transverse modulational instability in 2D, and are known to decay into vortices [45]. However, as was predicted in Ref. [19], sufficiently weak gray solitons can decay to *dark lumps* satisfying an effective KPI equation. This result suggests that, to observe dark lumps, one only need to embed a shallow dark soliton (like the ones we considered herein) into a 2D space, e.g., in a planar waveguide; then, the transverse instability will set in, and dark lump solitons will emerge. Finally, regarding the ring solitons, as mentioned above, they have already been observed in a variety of experiments (see, e.g., Ref. [46] and the review [45]) and, thus they can readily be created, e.g., in thermal media or in nematic liquid crystals. Thus, a variety of patterns that can be observed in water may also emerge in optics.

The obtained results relied on the formal reduction of the nonlocal NLS model to the KP (cKP) equation. It would be interesting to investigate if other types of nonlocality, arising, e.g., in the context of chromium Bose-Einstein condensates [47], or in defocusing colloidal media [48] can support relevant soliton states. Such studies are in progress and pertinent results will be presented elsewhere.

Author details

Georgios N. Koutsokostas[1*], Theodoros P. Horikis[2], Dimitrios J. Frantzeskakis[1], Nalan Antar[3] and İlkay Bakırtaş[3]

1 Department of Physics, University of Athens, Panepistimiopolis, Zografos, Athens 15784, Greece

2 Department of Mathematics, University of Ioannina, Ioannina 45110, Greece

3 Department of Mathematics, Istanbul Technical University, Maslak 34469, Istanbul, Turkey

*Address all correspondence to: koutsokwstasgewrgios@gmail.com

References

[1] Infeld E, Rowlands G. Nonlinear Waves, Solitons, and Chaos. Cambridge University Press; Cambridge, 1990.

[2] Dauxois T, Peyrard M. Physics of Solitons. Cambridge University Press; Cambridge, 2006.

[3] Ablowitz MJ, Clarkson PA. Solitons, nonlinear evolution equations and inverse scattering. Cambridge University Press; Cambridge, 1991.

[4] Ablowitz MJ. Nonlinear dispersive waves: Asymptotic analysis and solitons. Cambridge University Press; Cambridge, 2011.

[5] Ablowitz MJ, Baldwin DE. Nonlinear shallow ocean-wave soliton interactions on flat beaches. Phys Rev E. 2012;86: 036305.

[6] Kadomtsev BB, Petviashvili VI. On the stability of solitary waves in weakly dispersing media. Sov Phys Dokl. 1970; 15:539–541.

[7] Miles JW. Obliquely interacting solitary waves. J Fluid Mech. 1977;79: 157–169.

[8] Miles JW. Resonantly interacting solitary waves. J Fluid Mech. 1977;79: 171–179.

[9] Newell AC, Redekopp LG. Breakdown of Zakharov-Shabat Theory and Soliton Creation. Phys Rev Lett. 1977;38:377–380.

[10] Ohkuma K, Wadati M. The Kadomtsev-Petviashvili Equation: the Trace Method and the Soliton Resonances. J Phys Soc Jpn. 1983;52: 749–760.

[11] Biondini G, Kodama Y. On a family of solutions of the Kadomtsev-Petviashvili equation which also satisfy the Toda lattice hierarchy. J Phys A: Math Gen. 2003;36:10519.

[12] Biondini G, Chakravarty S. Soliton solutions of the Kadomtsev-Petviashvili II equation. J Math Phys. 2006;47: 033514.

[13] Chakravarty S, Kodama Y. Classification of the line-soliton solutions of KPII. J Phys A: Math Theor. 2008;41:275209.

[14] Chakravarty S, Kodama Y. Soliton Solutions of the KP Equation and Application to Shallow Water Waves. Stud Appl Math. 2009;123:83–151.

[15] Chakravarty S, Lewkow T, Maruno KI. On the construction of the KP line-solitons and their interactions. Applicable Analysis. 2010;89:529–545.

[16] McDowell T, Osborne M, Chakravarty S, Kodama Y. On a class of initial value problems and solitons for the KP equation: A numerical study. Wave Motion. 2017;72:201–227.

[17] Kivshar YS, Agrawal GP. Optical Solitons: From Fibers to Photonic Crystals. Academic Press; New York, 2003.

[18] Kuznetsov EA, Turitsyn SK. Instability and collapse of solitons in media with a defocusing nonlinearity. JETP. 1988;67:1583–1588.

[19] Pelinovsky DE, Stepanyants YA, Kivshar YS. Self-focusing of plane dark solitons in nonlinear defocusing media. Phys Rev E. 1995;51:5016–5026.

[20] Kivshar YS, Pelinovsky DE. Self-focusing and transverse instabilities of solitary waves. Phys Rep. 2000;331: 117–195.

[21] Horikis TP, Frantzeskakis DJ. Light Meets Water in Nonlocal Media: Surface Tension Analogue in Optics. Phys Rev Lett. 2017;118:243903.

[22] Johnson RS. Water waves and Korteweg-de Vries equations. J Fluid Mech. 1980;97:701–719.

[23] Johnson RS. A modern introduction to the mathematical theory of water waves. Cambridge University Press; 1997.

[24] Benney DJ, Luke JC. On the interactions of permanent waves of finite amplitude. J Math and Phys. 1964; 43:309–313.

[25] Rotschild C, Cohen O, Manela O, Segev M, Carmon T. Solitons in nonlinear media with an infinite range of nonlocality: first observation of coherent elliptic solitons and of vortex-ring solitons. Phys Rev Lett. 2005;95: 213904.

[26] Krolikowski W, Bang O, Nikolov NI, Neshev D, Wyller J, Rasmussen JJ, et al. Modulational instability, solitons and beam propagation in spatially nonlocal nonlinear media. J Opt B: Quantum Semiclass Opt. 2004;6:S288–S294.

[27] Ghofraniha N, Conti C, Ruocco G, Trillo S. Shocks in nonlocal media. Phys Rev Lett. 2007;99:043903.

[28] Conti C, Fratalocchi A, Peccianti M, Ruocco G, Trillo S. Observation of a gradient catastrophe generating solitons. Phys Rev Lett. 2009;102: 083902.

[29] Litvak AG, Mironov VA, Fraiman GM, Yunakovskii AD. Thermal self-effect of wave beams in a plasma with a nonlocal nonlinearity. Sov J Plasma Phys. 1975;1:60–71.

[30] Yakimenko AI, Zaliznyak YA, Kivshar YS. Stable vortex solitons in nonlocal self-focusing nonlinear media. Phys Rev E. 2005;71:065603(R).

[31] Conti C, Peccianti M, Assanto G. Route to nonlocality and observation of accessible solitons. Phys Rev Lett. 2003; 91:073901.

[32] Assanto G. Nematicons: Spatial Optical Solitons in Nematic Liquid Crystals. New Jersey: Wiley-Blackwell; 2012.

[33] Ablowitz MJ, Clarkson PA. Solitons, nonlinear evolution equations and inverse scattering. Cambridge University Press; Cambridge, 1991.

[34] Horikis TP. Small-amplitude defocusing nematicons. J Phys A: Math Theor. 2015;48:02FT01.

[35] Horikis TP, Frantzeskakis DJ. Ring dark and antidark solitons in nonlocal media. Opt Lett. 2016;41:583–586.

[36] Ablowitz MJ, Segur H. Solitons and the inverse scattering transform. SIAM; 1981.

[37] Hirota R. Exact solutions to the equation describing “cylindrical solitons”. Phys Lett A. 1979;71:393–394.

[38] Johnson RS. A note on an asymptotic solution of the cylindrical Korteweg-de Vries equation. Wave Motion. 1999;30:1–16.

[39] Ko K, Kuehl HH. Cylindrical and spherical Korteweg-deVries solitary waves. Phys Fluids. 1979;22:1343–1348.

[40] Kivshar YS, Yang X. Ring dark solitons. Phys Rev E. 1994;50:R40–R43.

[41] Frantzeskakis DJ, Malomed BA. Multiscale expansions for a generalized cylindrical nonlinear Schrödinger equation. Phys Lett A. 1999;264: 179–185.

[42] Dreischuh A, Neshev D, Paulus GG, Grasbon F, Walther H. Ring dark solitary waves: Experiment versus theory. Phys Rev E. 2002;66:066611.

[43] Nistazakis HE, Frantzeskakis DJ, Malomed BA, Kevrekidis PG. Head-on

collisions of ring dark solitons. Phys Lett A. 2001;285:157–164.

[44] Coskun TH, Christodoulides DN, Kim YR, Chen Z, Soljacic M, M S. Bright Spatial Solitons on a Partially Incoherent Background. Phys Rev Lett. 2000;84: 2374–2377.

[45] Kivshar YS, Luther-Davies B. Dark optical solitons: physics and applications. Phys Rep. 1998;298:81–197.

[46] Dreischuh A, Neshev D, Paulus GG, Grasbon F, Walther H. Ring dark solitary waves: Experiment versus theory. Phys Rev E. 2002;66:066611.

[47] Lahaye T, Menotti C, Santos L, Lewenstein M, Pfau T. The physics of dipolar bosonic quantum gases. Rep Prog Phys. 2009;72:126401.

[48] An X, Marchant TR, Smyth NF. Optical dispersive shock waves in defocusing colloidal media. Physica D. 2017;342:45–56.